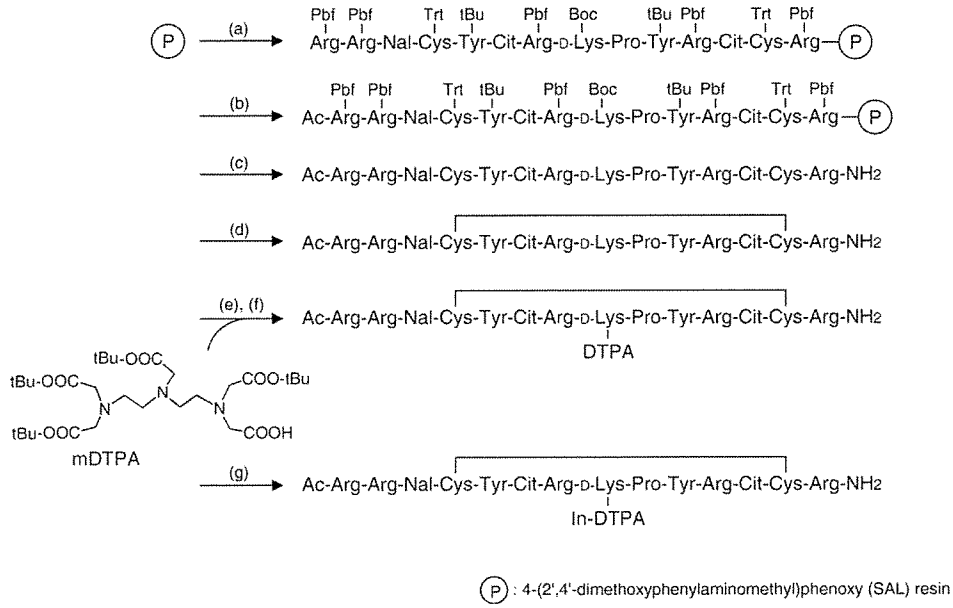

Fig. 2. Synthesis of In-DTPA-Ac-TZ14011. Reagents: (a) stepwise elongation; (b) acetic anhydride, pyridine; (c) trifluoroacetic acid, thioanisole, *m*-cresol, 1,2-ethanedithiol; (d) air oxidation; (e) *N*-hydroxysuccinimide, *N*,*N*-dicyclohexylcarbodiimide; (f) trifluoroacetic acid; (g) $InCl_3 \cdot 4H_2O$.

purification by RP-HPLC was carried out with a Hydrosphere C18 column (4.6×250 mm, YMC, Kyoto, Japan) eluted with 17% acetonitrile in 0.1% aqueous TFA at a flow rate of 1 ml/min. Fractions containing the peptide were collected, and the solvent was removed by lyophilization to afford In-DTPA-Ac-TZ14011 as a white powder. IS-MS calcd for $InC_{106}H_{161}N_{38}O_{28}S_2$ $[M+H^+]$: *m/z* 2594.2, found: *m/z* 2594.3.

2.3. Synthesis of ^{111}In-DTPA-Ac-TZ14011

$^{111}InCl_3$ (3.7 MBq) in 0.02N HCl (100 μl) was added to DTPA-Ac-TZ14011 (10 μg) in 0.1 M acetic acid (200 μl), and the mixture was incubated for 30 min at room temperature. Then, ^{111}In-DTPA-Ac-TZ14011 was separated from DTPA-Ac-TZ14011 by RP-HPLC under the same conditions used for the purification of In-DTPA-Ac-TZ14011. The radiochemical purity of ^{111}In-DTPA-Ac-TZ14011 was determined by TLC, CAE and RP-HPLC.

2.4. Binding assay

The binding assay was performed according to the procedure of Hesselgesser et al. [20] with a slight modification. The stable CXCR4-transfected Chinese hamster ovary (CHO) cell lines were prepared by transfection with cDNA encoding alanine scanning mutants in pcDNA3 (Invitrogen, Carlsbad, CA, USA) using lipofectamine (GIBCO, Rockville, MD, USA) and selection in neomycin (G418 500 mg/ml; GIBCO). The expression of CXCR4 on the surface of each transfectant was measured by flow cytometry. CXCR4-transfected CHO cell lines were suspended in the binding buffer (Ham's F-12 containing 20 mM HEPES and 0.5% BSA) and placed in siliconized tubes (5×10^5 cells/120 μl/tube). Binding reactions were performed on ice for 1 h in the presence of [^{125}I]SDF-1α (PerkinElmer Life Sciences, Boston, MA, USA) and various concentrations of peptides. Cells were separated from the buffer by centrifugation through a dibutylphthalate/olive oil mixture. After removal of the water and oil layer, cell-associated radioactivity was measured. The 50% inhibitory concentration (IC_{50}) of peptides was determined based on inhibition of the binding of SDF-1α to CXCR4-transfected CHO cells.

2.5. Calcium fluorimetry

Calcium fluorimetry was performed as described previously [21]. CXCR4-transfected CHO cell lines were placed in wells of a microtiter tray (3×10^4 cells/100 μl/well) and incubated for 1 day at 37°C in a CO_2 incubator. The cells were loaded with 5 μM of Fura-2-AM (Dojindo Laboratories, Kumamoto, Japan), 2.5 mM probenecid (Sigma, St Louis, MO, USA) and 20 mM HEPES (pH 7.4) in Ham's F-12 (80 μl/well) for 1 h at 37°C. After the cells were incubated with various concentrations of T140 analogs for 3 min, recombinant human SDF-1α (PeproTech EC, London, UK) was added. Changes in intracellular Ca^{2+} concentrations were measured by a spectrofluorometer (96-well Fluorescence Drug Screening System, Hamamatsu Photonix, Hamamatsu, Japan) using a modified version of the Fura-2 method [22]. The IC_{50} of peptides was determined based on the inhibition of Ca^{2+} mobilization induced by SDF-1α through CXCR4.

2.6. Biodistribution study in tumor-bearing mice

Animal experiments were conducted in accordance with our institutional guidelines and were approved by the Kyoto University Animal Care Committee. Athymic nude BALB/c

mice (8 weeks old, female) were inoculated subcutaneously with CXCR4-expressing pancreatic carcinoma cells, AsPC-1 [23,24]. When tumors were approximately 0.5 cm in diameter, the animals were intravenously injected with ^{111}In-DTPA-Ac-TZ14011 (25–30 kBq). The biodistribution of radioactivity was monitored at 1, 6 and 24 h postinjection. Groups of five mice were used for the experiments. Organs of interest were excised and weighed, and the radioactivity counts were determined with a well counter (ARC380CL, Aloka, Tokyo, Japan). For the in vivo blocking experiment, mice were coinjected with Ac-TZ14011 (10 mg/kg).

2.7. Statistical analysis

Statistical analysis was performed by using the unpaired t-test. $P<.05$ was considered to be statistically significant.

3. Results and discussion

T140 and its analogs have one disulfide bond and maintain an antiparallel β-sheet structure connected by a type II′ β-turn with D-Lys^8-Pro^9 at the (i+1) and (i+2) positions, and the side chain of D-Lys^8 is distant from the pharmacophore for the antagonistic activity [14,15]. Therefore, we designed Ac-TZ14011 as a mother compound that contains the residues indispensable for the antagonistic activity and has a single amino group of D-Lys^8 for site-selective conjugation of DTPA (Fig. 1). In calcium fluorimetric assays, this compound showed strong inhibitory activity equal to that of T140 (Table 1). To assess the effect of the conjugation of In-DTPA with Ac-TZ14011 on the antagonistic activity toward CXCR4, nonradioactive In-DTPA-Ac-TZ14011 was synthesized (Fig. 2). In binding assays with CXCR4, In-DTPA-Ac-TZ14011 maintained strong inhibitory activity although its IC_{50} value was slightly larger than that of Ac-TZ14011 (Table 1). This result indicated the validity of the chemical design of In-DTPA-Ac-TZ14011 based on structure–activity relationships.

In RP-HPLC analyses, In-DTPA-Ac-TZ14011 and DTPA-Ac-TZ14011 showed well-separated peaks as shown in Fig. 3. After purification by RP-HPLC under the same conditions, ^{111}In-DTPA-Ac-TZ14011 was obtained with high radiochemical purity (over 96%) as determined by TLC, CAE and RP-HPLC. The radioactivity pharmacokinetics of ^{111}In-DTPA-Ac-TZ14011 was evaluated in nude mice bearing the CXCR4-expressing pancreatic carcinoma AsPC-1 (Table 2). ^{111}In-DTPA-Ac-TZ14011 showed a rapid clearance from the blood and a marked accumulation and retention in the liver, kidney and spleen. The accumulation of radioactivity was greater in the tumor than in the blood or muscle (Table 2). In mice, CXCR4 mRNA is highly expressed in various lymphoid tissues and cells such as spleen, thymus, lymph node, bone marrow and leukocytes [25,26]. Thus, since liver and spleen are concerned with the immune system, the accumulation of ^{111}In-DTPA-Ac-TZ14011 in these organs should be mediated by CXCR4-binding. In fact, coinjection of Ac-TZ14011 significantly reduced the accumulation in the liver by over one-tenth and in the spleen by over one-third. This marked reduction of radioactivity in the liver and spleen on the coinjection of Ac-TZ14011 caused the high levels of radioactivity in the blood and consequently increased the accumulation of radioactivity in organs which were small in size and/or did not take up much radioactivity (Table 2). The accumulation in the tumor was also increased by coinjection of Ac-TZ14011, but the tumor-to-blood and tumor-to-muscle ratios were significantly reduced (Table 2). Since there is very little or no CXCR4 in the muscle [26],

Table 1
Antagonistic activity of T140 derivatives

	IC_{50} (nM)	
	SDF-1α binding[a]	Ca^{2+} mobilization[b]
In-DTPA-Ac-TZ14011	7.9	ND[c]
Ac-TZ14011	1.2	2.6
T140	ND[c]	2.2

[a] Values are the concentrations for 50% inhibition of the binding of [^{125}I]SDF-1α to CXCR4.
[b] Values are the concentrations for 50% inhibition of Ca^{2+} mobilization induced by SDF-1á through CXCR4.
[c] Not determined.

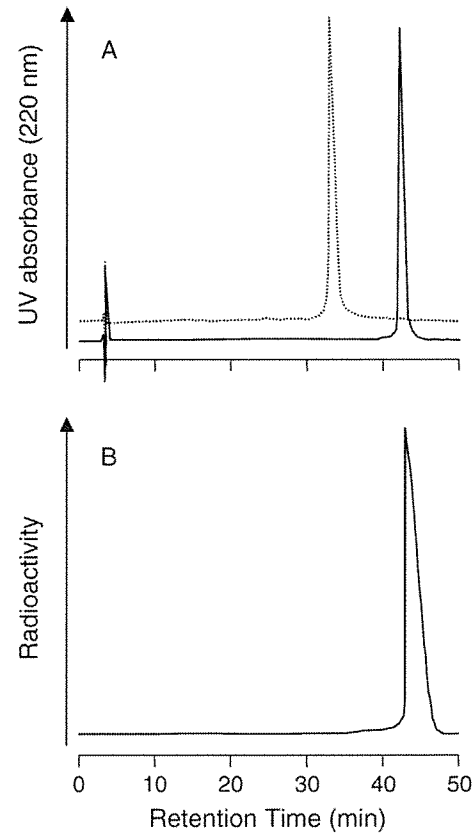

Fig. 3. Reversed-phase HPLC profiles of nonradioactive In-DTPA-Ac-TZ14011 (solid line), DTPA-Ac-TZ14011 (broken line) (A) and ^{111}In-DTPA-Ac-TZ14011 (B).

Table 2
Biodistribution of radioactivity after intravenous injection of ^{111}In-DTPA-Ac-TZ14011 in nude mice bearing pancreatic carcinoma, AsPC-1

	1 h	6 h	24 h	1 h+ Ac-TZ14011[a]
Blood[b]	0.39 (0.06)	0.05 (0.01)	0.03 (0.01)	2.06** (0.61)
Liver[b]	27.0 (2.9)	25.2 (2.0)	19.3 (2.5)	1.95** (0.25)
Kidney[b]	50.9 (4.3)	43.4 (6.3)	29.5 (5.7)	45.4 (6.8)
Spleen[b]	8.22 (0.70)	7.57 (0.54)	5.83 (0.99)	2.66** (1.21)
Pancreas[b]	0.15 (0.03)	0.05 (0.01)	0.05 (0.02)	1.07** (0.46)
Muscle[b]	0.17 (0.05)	0.07 (0.02)	0.07 (0.01)	1.35** (0.26)
Tumor[b]	0.51 (0.08)	0.20 (0.03)	0.14 (0.03)	1.70** (0.27)
T/B ratio[c]	1.31 (0.14)	4.05 (0.79)	5.65 (2.89)	0.88* (0.31)
T/M ratio[d]	3.17 (0.99)	4.43 (1.89)	3.23 (1.08)	1.31** (0.41)

Each value represents the mean (S.D.) for five animals.
[a] Coinjection with unlabeled Ac-TZ14011 (10 mg/kg).
[b] Expressed as % injected dose per gram.
[c] Tumor-to-blood ratio.
[d] Tumor-to-muscle ratio.
* $P<.05$, comparison between ^{111}In-DTPA-Ac-TZ14011 with or without unlabeled Ac-TZ14011 at 1 h.
** $P<.005$, comparison between ^{111}In-DTPA-Ac-TZ14011 with or without unlabeled Ac-TZ14011 at 1 h.

tumor-to-muscle ratios reflect target-to-nontarget ratios. Thus, the reduction in the tumor-to-muscle ratio caused by the coinjection of Ac-TZ14011 indicated that ^{111}In-DTPA-Ac-TZ14011 accumulated in the tumor through CXCR4. On the other hand, coinjection of Ac-TZ14011 did not alter the levels of ^{111}In-DTPA-Ac-TZ14011 in the kidney, suggesting a nonspecific accumulation. This is consistent with previous findings that CXCR4 mRNA levels expressed in the kidney were very low [25,26]. Recent studies indicated that an electrostatic interaction between positively charged peptides and the negatively charged surface of renal proximal tubular cells plays an important role in the reabsorption of peptides into proximal tubular cells [27–29]. Since five Arg residues are contained in the peptide ^{111}In-DTPA-Ac-TZ14011, the highly positive charge would cause a greater nonspecific accumulation in the kidney even compared to other ^{111}In-DTPA peptides [28,30,31]. Due to its accumulation in nontarget organs, ^{111}In-DTPA-Ac-TZ14011 may be unavailable as a radiopharmaceutical for screening small tumors, particularly in the kidneys and their surroundings.

It was reported that CXCR4 expression could be a powerful predictive factor for prognosis (recurrence, metastasis or survival rate) in colorectal cancer [32,33], malignant melanoma [34] and osteosarcoma [35]. Therefore, a CXCR4 imaging agent would be a new type of radiopharmaceutical for predicting the prognosis of cancer patients. CXCR4 also represents a novel target for tumor therapy, and some CXCR4 inhibitors have been investigated as anti-metastatic agents [36–39]. These agents showed positive effects in suppressing tumor metastasis; however, they would also have deleterious effects on normal physiological functions since CXCR4 plays a crucial role in numerous biological processes [2]. Therefore, in vivo imaging of CXCR4 expression could be a potential method for determining the dose of anti-metastatic agents and for monitoring their therapeutic efficacy.

In conclusion, we designed ^{111}In-DTPA-Ac-TZ14011 based on the structure–activity relationships of peptidic CXCR4 inhibitors. In-DTPA-Ac-TZ14011 showed strong inhibitory activity against the binding of CXCR4 to an endogenous ligand. Furthermore, the accumulation of ^{111}In-DTPA-Ac-TZ14011 in the CXCR4-expressing tumor was greater than that in the blood or muscle, being mediated by this receptor. These findings suggest that ^{111}In-DTPA-Ac-TZ14011 is a potential radiopharmaceutical for the imaging of CXCR4 expression in metastatic tumors in vivo for predicting the prognosis of cancer patients and for monitoring the therapeutic efficacy of anti-metastatic agents.

Acknowledgments

We are grateful to Nihon Medi-Physics (Nishinomiya, Japan) for the gift of $^{111}InCl_3$. This work was supported in part by a Grant-in-Aid for Cancer Research from the Ministry of Health, Labour and Welfare.

References

[1] Zlotnik A, Yoshie O. Chemokines: a new classification system and their role in immunity. Immunity 2000;12:121–7.
[2] Horuk R. Chemokine receptors. Cytokine Growth Factor Rev 2001;12:313–35.
[3] Feng Y, Broder CC, Kennedy PE, Berger EA. HIV-1 entry cofactor: functional cDNA cloning of a seven-transmembrane, G protein-coupled receptor. Science 1996;272:872–7.
[4] Müller A, Homey B, Soto H, Ge N, Catron D, Buchanan ME, et al. Involvement of chemokine receptors in breast cancer metastasis. Nature 2001;410:50–6.
[5] Taichman RS, Cooper C, Keller ET, Pienta KJ, Taichman NS, McCauley RS. Use of the stromal cell-derived factor-1/CXCR4 pathway in prostate cancer metastasis to bone. Cances Res 2002;62: 1832–7.
[6] Schrader AJ, Lechner O, Templin M, Dittmar KEJ, Machtens S, Mengel M, et al. CXCR4/CXCL12 expression and signaling in kidney cancer. Br J Cancer 2002;86:1250–6.
[7] Phillips RJ, Burdick MD, Lutz M, Belperio JA, Keane MP, Strieter RM. The stromal derived factor-1/CXCL12-CXC chemokine receptor 4 biological axis in non-small cell lung cancer metastases. Am J Respir Crit Care Med 2003;167:1676–86.
[8] Uchida D, Begum NM, Almofti A, Nakashiro K, Kawamata H, Tateishi Y, et al. Possible role of stromal-cell-derived factor-1/CXCR4 signaling on lymph node metastasis of oral squamous cell carcinoma. Exp Cell Res 2003;290:289–302.
[9] Masuda M, Nakashima H, Ueda T, Naba H, Ikoma R, Otaka A, et al. A novel anti-HIV synthetic peptide, T-22 ([Tyr^{5,12}Lys^{7}]-polyphemusin II). Biochem Biophys Res Commun 1992;189:845–50.
[10] Murakami T, Nakajima T, Koyanagi Y, Tachibana K, Fujii N, Tamamura H, et al. A small molecule CXCR4 inhibitor that blocks T cell line-tropic HIV-1 infection. J Exp Med 1997;186: 1389–93.
[11] Tamamura H, Arakaki R, Funakoshi H, Imai M, Otaka A, Ibuka T, et al. Effective lowly cytotoxic analogs of an HIV-cell fusion inhibitor, T22 ([Tyr^{5,12},Lys^{7}]-polyphemusin II). Bioorg Med Chem 1998;6:231–8.
[12] Tamamura H, Xu Y, Hattori T, Zhang X, Arakaki R, Kanbara K, et al. A low-molecular- weight inhibitor against the chemokine receptor

CXCR4: a strong anti-HIV peptide T140. Biochem Biophys Res Commun 1998;253:877–82.

[13] Tamamura H, Omagari A, Oishi S, Kanamoto T, Yamamoto N, Peiper SC, et al. Pharmacophore identification of a specific CXCR4 inhibitor, T140, leads to development of effective anti-HIV agents with very high selectivity indexes. Bioorg Med Chem Lett 2000;10:2633–7.

[14] Tamamura H, Sugioka M, Odagaki Y, Omagari A, Kan Y, Oishi S, et al. Conformational study of a highly specific CXCR4 inhibitor, T140, disclosing the close proximity of its intrinsic pharmacophores associated with strong anti-HIV activity. Bioorg Med Chem Lett 2001;11:359–62.

[15] Tamamura H, Sugioka M, Odagaki Y, Omagari A, Kan Y, Oishi S, et al. Corrigendum to "conformational study of a highly specific CXCR4 inhibitor, T140, disclosing the close proximity of its intrinsic pharmacophores associated with strong anti-HIV activity" [Bioorg. Med. Chem. Lett. 11 (2001) 359]. Bioorg Med Chem Lett 2001;11:2409.

[16] Tamamura H, Omagari A, Hiramatsu K, Gotoh K, Kanamoto T, Xu Y, et al. Development of specific CXCR4 inhibitors possessing high selectivity indexes as well as complete stability in serum based on an anti-HIV peptide T140. Bioorg Med Chem Lett 2001;11:1897–902.

[17] Tamamura H, Hiramatsu K, Kusano S, Terakubo S, Yamamoto N, Trent JO, et al. Synthesis of potent CXCR4 inhibitors possessing low cytotoxicity and improved biostability based on T140 derivatives. Org Biomol Chem 2003;1:3656–62.

[18] Arano Y, Uezono T, Akizawa H, Ono M, Wakisaka K, Nakayama M, et al. Reassessment of diethylenetriaminepentaacetic acid (DTPA) as a chelating agent for indium-111 labeling of polypeptides using a newly synthesized monoreactive DTPA derivative. J Med Chem 1996;39: 3451–60.

[19] Arano Y, Akizawa H, Uezono T, Akaji K, Ono M, Funakoshi S, et al. Conventional and high-yield synthesis of DTPA-conjugated peptide: application of a monoreactive DTPA to DTPA-D-Phe^1-octreotide synthesis. Bioconjug Chem 1997;8:442–6.

[20] Hesselgesser J, Liang M, Hoxie J, Greenberg M, Brass LF, Orsini MJ, et al. Identification and characterization of CXCR4 chemokine receptor in human T cell lines: ligand binding, biological activity, and HIV-1 infectivity. J Immunol 1998;160:877–83.

[21] Tamamura H, Omagari A, Hiramatsu K, Oishi S, Habashita H, Kanamoto T, et al. Certification of the critical importance of L-3-(2-naphthyl)alanine at position 3 of specific CXCR4 inhibitor, T140, leads to an exploratory performance of its downsizing study. Bioorg Med Chem 2002;10:1417–26.

[22] Grynkiewicz G, Poenie M, Tsien RY. A new generation of Ca^{2+} indicators with greatly improved fluorescence properties. J Biol Chem 1985;260:3440–50.

[23] Koshiba T, Hosotani R, Miyamoto Y, Ida J, Tsuji S, Nakajima S, et al. Expression of stromal cell-derived factor 1 and CXCR4 ligand receptor system in pancreatic cancer: a possible role for tumor progression. Clin Cancer Res 2000;6:3530–5.

[24] Mori T, Doi R, Koizumi M, Toyoda E, Ito D, Kami K, et al. CXCR4 antagonist inhibits stromal cell-derived factor 1-induced migration and invasion of human pancreatic cancer. Mol Cancer Ther 2004;3: 29–37.

[25] Nagasawa T, Nakajima T, Tachibana K, Iizasa H, Bleul CC, Yoshie O, et al. Molecular cloning and characterization of a murine pre-B-cell growth-stimulating factor/stromal cell-derived factor 1 receptor, a murine homolog of the human immunodeficiency virus 1 entry coreceptor fusin. Proc Natl Acad Sci U S A 1996;93:14726–9.

[26] Moepps B, Frodl R, Rodewald HR, Bsggiolini M, Gierschik P. Two murine homologues of the human chemokine receptor CXCR4 mediating stromal cell-derived factor 1α activation of G_{i2} are differentially expressed in vivo. Eur J Immunol 1997;27: 2102–12.

[27] de Jong M, Rolleman EJ, Bernard BF, Visser TJ, Bakker WH, Breeman WAP, et al. Inhibition of renal uptake of indium-111-DTPA-octreotide in vivo. J Nucl Med 1996;37:1388–92.

[28] Akizawa H, Arano Y, Mifune M, Iwado A, Saito Y, Mukai T, et al. Effect of molecular charges on renal uptake of ^{111}In-DTPA-conjugated peptides. Nucl Med Biol 2001;28:761–8.

[29] Akizawa H, Takimoto H, Saito M, Iwado A, Mifune M, Saito Y, et al. Effect of carboxylation of N-terminal phenylalanine of ^{111}In-DTPA (diethylenetriaminepentaacetic acid)-octreotide on accumulation of radioactivity in kidney. Biol Pharm Bull 2004;27:271–2.

[30] Bagutti C, Stolz B, Albert R, Bruns C, Pless J, Eberle AN. [^{111}In]-DTPA-labeled analogues of α-melanocyte-stimulating hormone for melanoma targeting: receptor binding in vitro and in vivo. Int J Cancer 1994;58:749–55.

[31] de Visser M, Janssen PJJM, Srinvasan A, Reubi JC, Waser B, Erion JL, et al. Stabilised ^{111}In-labelled DTPA- and DOTA-conjugated neurotensin analogues for imaging and therapy of exocrine pancreatic cancer. Eur J Nucl Med Mol Imaging 2003;30:1134–9.

[32] Schimanski CC, Schwald S, Simiantonaki N, Jayasinghe C, Gonner V, Wilsberg V, et al. Effect of chemokine receptors CXCR4 and CCR7 on the metastatic behavior of human colorectal cancer. Clin Cancer Res 2005;11:1743–50.

[33] Kim J, Takeuchi H, Lam ST, Turner RR, Wang HJ, Kuo C, et al. Chemokine receptor CXCR4 expression in colorectal cancer patients increases the risk for recurrence and for poor survival. J Clin Oncol 2005;23:2744–53.

[34] Scala S, Ottaiano A, Ascierto PA, Cavalli M, Simeone E, Giuliano P, et al. Expression of CXCR4 predicts poor prognosis in patients with malignant melanoma. Clin Cancer Res 2005;11:1835–41.

[35] Laverdiere C, Hoang BH, Yang R, Sowers R, Qin J, Meyers PA, et al. Messenger RNA expression levels of CXCR4 correlate with metastatic behavior and outcome in patients with osteosarcoma. Clin Cancer Res 2005;11:2561–7.

[36] Tamamura H, Hori A, Kanzaki N, Hiramatsu K, Mizumoto M, Nakashima H, et al. T140 analogs as CXCR4 antagonists identified as anti-metastatic agents in the treatment of breast cancer. FEBS Lett 2003;550:79–83.

[37] Liang Z, Wu T, Lou H, Yu X, Taichman RS, Lau SK, et al. Inhibition of breast cancer metastasis by selective synthetic polypeptide against CXCR4. Cancer Res 2004;64:4302–8.

[38] Takenaga M, Tamamura H, Hiramatsu K, Nakamura N, Yamaguchi Y, Kitagawa A, et al. A single treatment with micro-capsules containing a CXCR4 antagonist suppresses pulmonary metastasis of murine melanoma. Biochem Biophys Res Commun 2004;320:226–32.

[39] Smith MC, Luker KE, Garbow JR, Prior JL, Jackson E, Piwnica-Worms D, et al. CXCR4 regulates growth of both primary and metastatic breast cancer. Cancer Res 2004;64:8604–12.

HETEROCYCLES, Vol. 70, 2006, pp. . © The Japan Institute of Heterocyclic Chemistry
Received, 29th September, 2006, Accepted, 15th November, 2006, Published online, 17th November, 2006. COM-06-S(W)51

PHOTOCHEMICAL SYNTHESIS OF POLYCYCLIC PYRIMIDINES THROUGH THE ACID CATALYZED CYCLOADDITION OF 6-CHLORO-1-METHYLURACIL TO METHYL SUBSTITUTED BENZENES

Kazue Ohkura,*[,a] Takeshi Yamaguchi,[a] Ken-ichi Nishijima,[a] Yuji Kuge,[b] and Koh-ichi Seki[b]

[a] Faculty of Pharmaceutical Sciences, Health Sciences University of Hokkaido, Ishikari-Tobetsu, Hokkaido 061-0293, Japan
[b] Graduate School of Medicine, Hokkaido University, Kita-15, Nishi-7, Kita-ku, Sapporo 060-0815, Japan
E-mail: ohkura@hoku-iryo-u.ac.jp

Abstract – UV-irradiation of 6-chloro-1-methyluracil with benzene in the presence of TFA resulted in 1,2-cycloaddition and susequent elimination of HCl gave a cyclooctapyrimidine-2,4-dione. Similar acid catalyzed photoreaction with substituted benzenes bearing two or three methyl groups afforded the corresponding cyclooctapyrimidines and two novel pentacyclic compounds, 9,11-diazapentacyclo[6.4.0.0^{1,3}.0^{2,5}.0^{4,8}]dodecanes and 9.11-diazapentacyclo[6.4.0.0^{1,3}.0^{2,6}.0^{4,8}]dodcanes, in fair yields.

Recently, photoreaction of nucleic bases has been received much attention from both organic chemistry and biological perspectives.[1] During the course of our continuing studies on the photochemical modification of the pyrimidine ring, we have previously reported that the acid catalyzed photoreaction of 6-chloro-1,3-dimethyluracil (6-ClDMU) with benzene derivatives proceeds by way of 1,2-cycloaddition to give cyclooctapyrimidines.[2] Certain cyclooctapyrimidines were further converted into various novel valence isomers,[3-5] by way of a variety of electrocyclic pathways depending on the reaction conditions and substituents on the cycloadducts. These reactions however, have been carried out with both *N*1 and *N*3 methyl capped uracils. Taking the biological importance of the *N*3-H moiety of the pyrimidine ring into consideration, the presence of a non-protected *N*3-H function of the pyrimidine ring

---

This paper is dedicated to Professor Steven M. Weinreb on the occasion of his 65th birthday.

may represent a significant pharmacophore for the development of useful chemotherapeutics. We intended to extend this photoreaction to 6-chloro-1-methyluracil (**1**) bearing an *N*3-H function. In the present paper, we describe that the photoreaction of **1** with benzene and its methyl derivatives in the presence of TFA successfully effected cycloaddition to give NH free polycyclic pyrimidines.

UV-irradiation of a solution of 6-chloro-1-methyluracil (**1**) in benzene (**2a**) with a 500 W high-pressure mercury lamp in a degassed Pyrex tube (λ>300 nm) for 16 h afforded 1-methyl-6-phenyluracil (**3a**) in low yield (3%), together with large amount of unreacted **1**. In contrast, the addition of TFA to the solution gave rise to the formation of 1-methylcyclooctapyrimidine-2,4-dione (**4a**) in appreciable yield (70%, based on 73% **1** consumed), while the substitution reaction was significantly attenuated (3%) (Scheme 1).

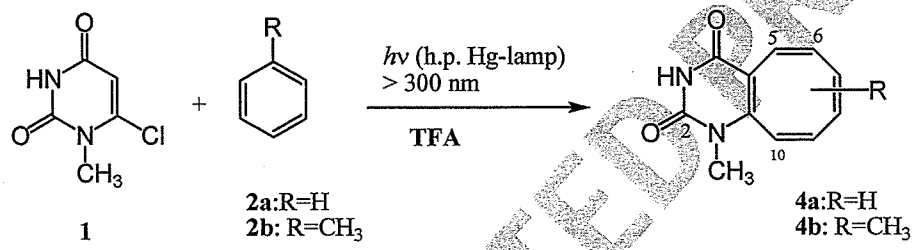

1 **2a**:R=H **2b**: R=CH_3 **4a**:R=H **4b**: R=CH_3

Scheme 1

The structural assignment of **4a** was made on the basis of detailed MS and the NMR spectroscopic studies. The coupling constants for the vinyl protons of **4a**, $J_{5,6}$, $J_{7,8}$, $J_{9,10}$ = 11.5 Hz, and $J_{6,7}$, $J_{8,9}$, = 3.5-4 Hz, revealed the configurations to be all *cis*.

The photoreaction with toluene (**2b**) under the above conditions afforded five isomeric 1,*n*-dimethyl-cyclooctapyrimidines (*n*=6,7,8,9,10) in fair yield (**4b**$_6$:23%, **4b**$_7$: 16%, **4b**$_8$: 25%, **4b**$_9$: 7%, **4b**$_{10}$: 18%) (Scheme1). The structural assignments, including the stereochemistry of **4b** were made on the basis of the similarity to **4a** in their ^{1}H-NMR spectroscopic data. Methyl substituted sites on the cycloocta-tetraene moiety were determined by NOE experiments.

Thus, analogous to the case of the reaction with 6-ClDMU and **2a,b**, UV excitation of **1** undergoes 1,2-cycloaddition with **2a,b** to produce cyclooctapyrimidines *via* the concomitant elimination of hydrogen chloride which is then followed by an electrocyclic ring opening reaction.

We then investigated the photoreaction with *p*-xylene (**2c**) under the same conditions. HPLC separation of the reaction mixture afforded three types of cycloadducts as single regioisomers namely, 1, 7,10-trimethylcyclooctapyrimidine-2,4-dione (**4c**) in 31% yield along with two novel pentacyclic compounds, 6-methylene-3,9-dimethyl-9,11-diazapentacyclo[6.4.0.0^{1,3}.0^{2,5}.0^{4,8}]dodecane-10,12-dione (**5c**) and 5-methylene-2,9-dimethyl-9,11-diazapentacyclo[6.4.0.0^{1,3}.0^{2,6}.0^{4,8}]dodecane-10,12-dione (**6c**)

in 15% and 13 % yield respectively. Conversely, the reaction with toluene gave the cyclooctapyrimidines with poor regioselectivity (Scheme 2).

The structures of **5c** and **6c** were determined by comparison with the NMR data for *N*3-methyl penta-

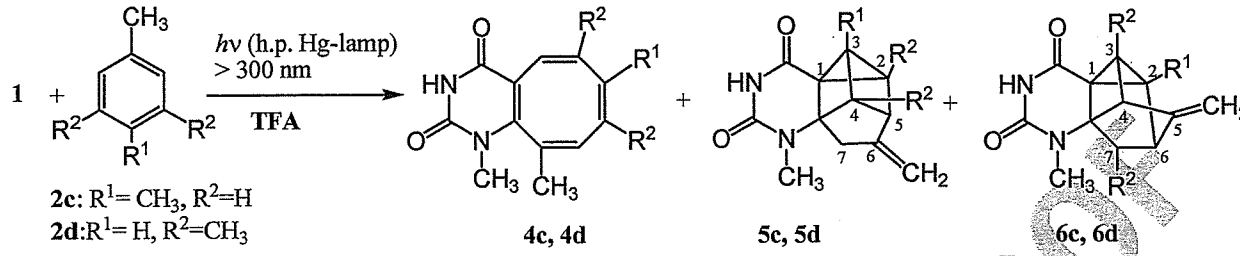

Scheme 2

cyclic derivatives which had given X-ray crystallographic data in detail.[6] The ^{1}H and ^{13}C-nmr spectra including ^{13}C-^{1}H COSY showed signals due to two methyl groups, two methylene groups, three methine groups and six quaternary carbon atoms. HMBC spectrum and NOE experiments provided the information to enable us to construct pentacyclic compounds consisting of 3, 4, 4, and 5-membered rings for **5c** and 3, 4, 5, and 5-membered rings for **6c**.

Similarly the photoreaction with mesitylene (**2d**) afforded 1,6,8,10-tetramethyl-cyclooctapyrimidine-2,4-dione (**4d**) (21%) and the two pentacyclic compounds, 6-methylene-2,4,9-trimethyl-9,11-diazapentacyclo[6.4.0.0^{1,3}.0^{2,5}.0^{4,8}]dodecane-10,12-dione (**5d**) (18%) and 5-methylene-3,7,9-trimethyl-9,11-diazapentacyclo[6.4.0.0^{1,3}.0^{2,6}.0^{4,8}] dodecane-10,12-dione (**6d**) (8%) (Scheme 2).

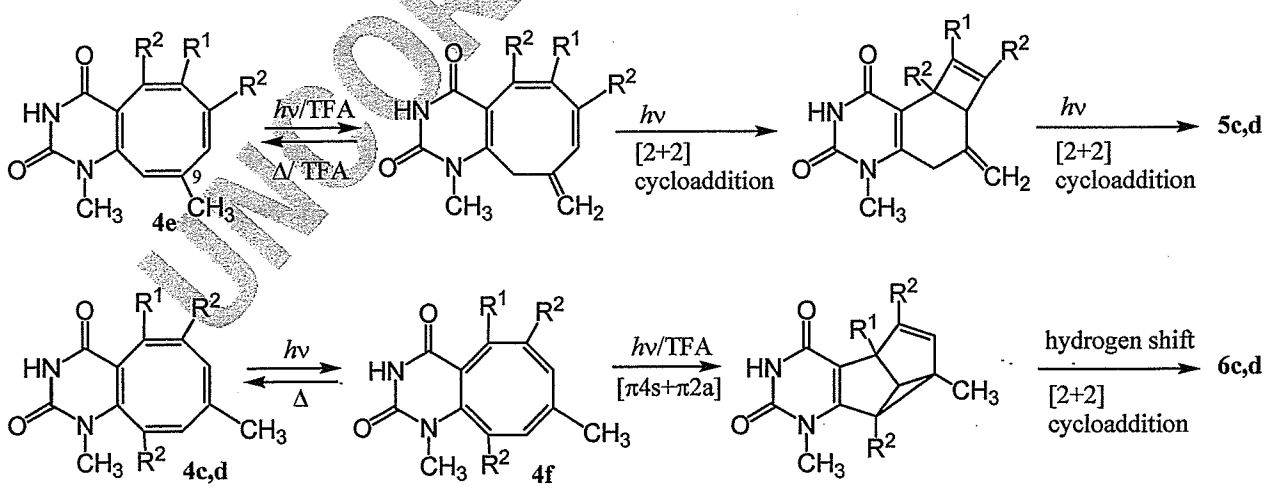

Scheme 3

The reaction pathway for the formation of the pentacyclic compound is inferred on the basis of the established pathway[7] for the formation of *N*3-methyl derivative respectively as depicted in Scheme 3. It

is suggested that compound **5** could be derived from 9-methylcyclooctapyrimidine (**4e**) *via* a multi-step transformation starting with a [1,3] sigmatropic rearrangement of 9-methyl group followed by subsequent double [2 + 2] cycloaddition processes. The formation of compound **6** can be explained by the rearrangement of cyclooctapyrimidine tautomer (**4f**) involving a [π4s +π2a] process.

These results provide the first example of the formation of various cycloadducts between *N*3-H chlorouracil and benzenes. Interestingly in this reaction methyl substituents on the benzene ring are effective auxiliaries in achieving subsequent electrocyclic rearrangement of photoadducts including forming highly strained pentacyclic cage compounds.

It is noteworthy that reactions involving *N*3 free 6-chlororouracil in place of dimethyluracil derivatives, would provide synthons for the synthesis of singular polycyclic systems including a *N*3 non-substituted pyrimidine ring.

EXPERMENTAL

NMR spectra were measured with a JEOL JNM-EA500 (500 MHz) spectrometer, and ^{1}H-NMR chemical shifts are given on the δ (ppm) scale based on those of the signals of solvents. MS spectra and high-resolution MS (HRMS) spectra were recorded with LEOL JMS-FABmate (EI). Reverse-phase liquid chromatography (RP-HPLC) was carried out on a Shim-pac PREP-ODS (25 cm x 20 mm *i.d.*) (Shimadzu) with aqueous methanol, using a Shimadzu LC-6A apparatus with monitoring at 254 nm. Silica gel LC (Si-HPLC) was conducted on a Shim-pac PREP-Sil (H) (25 cm x 20 mm *i.d.*) (silica gel), using the same apparatus. UV-Irradiation was carried out externally with a 500 W high-pressure mercury (h. p. Hg) lamp (Eiko-sha, Osaka) in a degassed Pyrex tube (> 300 nm) on a merry-go-round apparatus.

Photoreaction of 1 with 2 in the presence of TFA----- A solution of **1** (56 mg, 0.35 mmol) and TFA (10 equiv. mol: 260 µl) in benzenes (**2a-d**) (100 mL) was put portion-wise (10 mL each) into ten degassed Pyrex tubes and irradiated externally at room temperature for 16 h.

Typical procedure for the isolation of the cycloadduct----- After the photoreaction according to the general procedure, the reaction mixtures in several Pyrex tubes were put together, and evaporated *in vacuo*. The residual oil was passed through a short column of silica gel with AcOEt. The eluate was submitted to HPLC with following solvent systems; 30% MeOH-H_2O on RP-HPLC for **4a**, 15% AcOEt-hexane on Si-HPLC for **4b**, **4d**, **5d**, and **6d**, and 25% AcOEt- hexane on Si-HPLC for **4c**, **5c**, and **6c**.

1-Methylcyclooctapyrimidine-2,4-dione(4a): Yellow crystals, mp 243-246 °C (*i*-PrOH). ^{1}H–NMR

(C_6D_6) δ; 2.45 (3H, s, N^1-CH_3), 4.92 (1H, d, *J*=11.5 Hz, H-10), 5.41 (1H, dd, *J*=11.5, 3.5 Hz, H-9), 5.47 (1H, dd, *J*=11.5, 3.5 Hz, H-8), 5.58 (1H, dd, *J*=11.5, 4.0 Hz, H-7), 5.66 (1H, dd, *J*=11.5, 4.0 Hz, H-6), 6.24 (1H, d, *J*=11.5 Hz, H-5), 9.13 (1H, brs, N^3-H). NOE; H-10 with N^1-CH_3, H-9; H-5 with H-6; N^1-CH_3 with H-10. ^{13}C-NMR (C_6D_6); 30.47 (N^1-CH_3), 110.83 (4a), 125.74 (10), 127.55 (5), 129.33 (9), 130.79 (6), 133.05 (7), 135.39 (8), 149.16 (10a), 150.68 (2), 161.00 (4). MS *m/z* (%):202 (M^+, 100), 159 (55), 131 (42), 116 (32). *Anal.* Calcd for $C_{11}H_{10}N_2O_2$: C, 65.34; H, 4.98; N, 13.85. Found: C, 65.27; H, 4.99; N, 13.77.

1,6-Dimethylcyclooctapyrimidine-2,4-dione(4b$_6$): Yellow crystals, mp 220-223 °C (acetone). ^{1}H-NMR($CDCl_3$) δ; 1.86 (3H, s, C^6-CH_3), 3.28 (3H, s, N^1-CH_3), 5.89 (1H, s, H-5), 5.94 (1H, dd, *J*=11.5, 3.5 Hz, H-8), 6.01 (1H, d, *J*=11.5 Hz, H-7), 6.01 (1H, d, *J*=11.5 Hz, H-10), 6.31 (1H, dd, *J*=11.5, 3.5 Hz, H-9), 8.38 (1H,brs,N^3-H). NOE; H-10 with N^1-CH_3, H-9; H-9 with H-10, H-8; H-8 with H-9, H-7; H-7 with H-8, C^6-CH_3; C^6-CH_3 with H-7, H-5. ^{13}C-NMR($CDCl_3$) δ; 23.45 (C^6-CH_3), 31.88 (N^1-CH_3), 112.50 (4a), 121.63 (5), 125.56 (10), 127.86 (8), 136.44 (7), 136.93 (9), 140.93 (6), 149.79 (10a), 151.03 (2), 161.79 (4). MS *m/z* (%):216 (M^+, 100), 201 (11), 173 (38), 158 (18), 145 (39), 115 (14), 104 (18). HRMS; Calcd for $C_{12}H_{12}N_2O_2$: 216.0899. Found: 216.0902.

1,7-Dimethylcyclooctapyrimidine-2,4-dione(4b$_7$): Yellow crystals, mp 227-230 °C (*i*-PrOH). ^{1}H-NMR($CDCl_3$) δ; 1.78 (3H, s, C^7-CH_3), 3.28 (3H, s, N^1-CH_3), 5.74 (1H, m, H-8), 5.92 (1H, d, *J*=11.5 Hz, H-10), 5.97 (1H, d, *J*=11.5 Hz, H-6), 6.09 (1H, d, *J*=11.5 Hz, H-5), 6.27 (1H, dd, *J*=11.5, 3.5 Hz, H-9), 8.64 (1H, brs, N^3-H9). NOE; H-10 with N^1-CH_3, H-9; H-9 with H-10, H-8; H-8 with H-9, C^7-CH_3; C^7-CH_3 with H-8, H-6. ^{13}C-NMR ($CDCl_3$); 23.38 (C^7-CH_3), 31.80 (N^1-CH_3), 111.51 (4a), 124.47 (10), 124.90 (8), 124.93 (5), 135.49 (6), 137.91 (9), 141.83 (7), 150.63 (10a), 151.05 (2), 161.51 (4). MS *m/z* (%):216 (M^+, 100), 201 (15), 173 (27), 158 (18), 145 (33), 130 (22), 115 (9), 104 (22). *Anal.* Calcd for $C_{12}H_{12}N_2O_2$ C, 66.65; H, 5.59; N, 12.96. Found: C, 65.90; H, 5.52; N, 12.51.

1,8-Dimethylcyclooctapyrimidine-2,4-dione(4b$_8$): Yellow crystals, mp 207-210 °C (*i*-PrOH). ^{1}H-NMR($CDCl_3$) δ; 1.82 (3H, s, C^8-CH_3), 3.29 (3H, s, N^1-CH_3), 5.77 (1H, m, H-7), 5.93 (1H, d, *J*=11.5 Hz, H-10), 6.00 (1H, dd, *J*=11.5, 3.5 Hz, H-6), 6.10 (1H, d, *J*=11.5 Hz, H-5), 6.23 (1H, d, *J*=11.5 Hz, H-9). NOE; H-10 with N^1-CH_3, H-9; H-9 with H-10, C^8-CH_3; C^8-CH_3 with H-9, H-7; H-7 with C^8-CH_3, H-6; H-6 with H-7, H-5; N^1-CH_3 with H-10. ^{13}C-NMR ($CDCl_3$) δ; 22.48 (C^8-CH_3), 31.73 (N^1-CH_3), 111.60 (4a), 123.73 (10), 125.72 (5), 127.85 (7), 133.03 (6), 138.37 (8), 140.02 (9), 150.17 (10a), 151.26 (2), 161.77 (4). MS *m/z* (%):216 (M^+, 100), 201 (11), 176 (23), 173 (26), 158 (14), 145 (37), 144 (34), 130 (32), 115 (12), 104 (30). HRMS; Calcd for $C_{12}H_{12}N_2O_2$: 216.0899. Found: 216.0895.

1,9-Dimethylcyclooctapyrimidine-2,4-dione(4b$_9$): Yellow crystals, mp 245-247 °C (acetone). ^{1}H-

NMR($CDCl_3$) δ; 1.92 (3H, s, C^9-CH_3), 3.28 (3H, s, N^1-CH_3), 5.75 (1H, s, H-10), 5.94-6.00 (2H, m, H-7 and H-8), 6.06 (1H, dd, *J*=10.9, 3.5 Hz, H-6), 6.18 (1H, d, *J*=10.9 Hz, H-5), 8.43 (1H, brs, N^3-H). NOE; H-10 with N^1-CH_3, C^9-CH_3; C^9-CH_3 with H-10, H-8; H-6 with H-7, H-5; N^1-CH_3 with H-10. ^{13}C-NMR ($CDCl_3$) δ; δ; 23.90 (C^9-CH_3), 31.91 (N^1-CH_3), 111.13 (4a), 120.60 (10), 127.13 (5), 131.14 (8), 132.21 (6), 133.07 (7), 146.29 (9), 150.87 (10a), 151.15 (2), 161.69 (4). MS *m/z* (%):216 (M^+, 100), 201 (13), 176 (5), 173 (30), 158 (11), 130 (24), 115 (11), 104 (15). HRMS; Calcd for $C_{12}H_{12}N_2O_2$: 216.0899. Found: 216.0903.

1,10-Dimethylcyclooctapyrimidine-2,4-dione(4b$_{10}$): Orange oil. ^{1}H-NMR($CDCl_3$) δ; 1.94 (3H, s, C^{10}-CH_3), 3.27 (3H, s, N^1-CH_3), 5.96 (1H, dd, *J*=10.9, 3.5 Hz, H-7), 6.02 (2H, m, H-8 and H-9), 6.06 (1H, dd, *J*=10.9, 2.3 Hz, H-6), 6.28 (1H, d, *J*=10.9 Hz, H-5). NOE; C^{10}-CH_3 with N^1-CH_3, H-9; H-6 with H-5, H-7; N^1-CH_3 with C^{10}-CH_3. ^{13}C-NMR ($CDCl_3$) δ; 21.68 (C^{10}-CH_3), 32.62 (N^1-CH_3), 110.51 (4a), 126.38 (5), 130.40 (8), 132.01 (7), 132.09 (9), 132.35 (6), 133.82 (10), 151.75 (10a), 153.90 (2), 161.88 (4). MS *m/z* (%):216 (M^+, 100), 201 (17), 176 (6), 173 (32), 158 (28), 145 (37), 115 (14), 104 (23). HRMS; Calcd for $C_{12}H_{12}N_2O_2$: 216.0899. Found: 216.0899.

1,7,10-Trimethylcyclooctapyrimidine-2,4-dione(4c): Colorless crystals. mp 245-247 °C (*i*-PrOH). ^{1}H-NMR((acetone-d_6)) δ; 1.68 (3H, s, C^7-CH_3), 1.91 (3H, s, C^{10}-CH_3), 3.19 (3H, s, N^1-CH_3), 5.81 (1H, m, H-8), 5.91 (1H, brd, *J*=11.5 Hz, H-6), 6.00 (1H, m, H-9), 6.12 (1H, d, *J*=11.5 Hz, H-5). NOE; H-9 with C^{10}-CH_3, H-8; C^7-CH_3 with H-8, H-6; H-6 with C^7-CH_3, H-5; N^1-CH_3 with C^{10}-CH_3. ^{13}C-NMR ($CDCl_3$) (acetone-d_6) δ; 20.65 (C^{10}-CH_3), 22.25 (C^7-CH_3), 31.85 (N^1-CH_3), 109.89 (4a), 125.42 (5), 125.87 (8), 132.42 (9),133.23 (10), 134.22 (6), 139.57 (7), 151.50 (2), 153.82 (10a), 161.44 (4). MS *m/z* (%):230 (M^+, 100), 215 (27), 190 (19), 187 (13), 144 (37), 129 (6). *Anal.* Calcd for $C_{13}H_{14}N_2O_2$ C, 67.81; H, 6.13; N, 12.17. Found: C, 67.66; H, 6.13; N, 12.15.

9,11-Diaza-3,9-dimethyl-6-methylenepentacyclo[6.4.0.0^{1,3}.0^{2,5}.0^{4,8}]dodecane-10,12-dione(5c): colorless crystals. mp 215-217 °C (*i*-PrOH). ^{1}H-NMR ($CDCl_3$) δ; 1.48 (3H, s, C^3-CH_3), 2.45 (1H, dt, *J*=16.9, 2.6 Hz, H-7b), 2.55 (1H, dt, *J*=16.9, 2.0 Hz, H-7a), 2.80(1H, t, *J*=4.6 Hz, H-4), 2.86 (1H, dd, *J*=4.6, 2.9 Hz,H-2), 2.96 (3H, s, N^9-CH_3), 3.68 (1H, dd, *J*=4.6, 2.9 Hz, H-5), 4.75 (1H, brs, C^6=CHb), 4.91 (1H, t-like, C^6=CHa), 7.48 (1H, brs, N^{11}-H). NOE; H-2 with H-5, C^3-CH_3; H-4 with C^3-CH_3, N^9-CH_3, H-5; H-5 with H-7a, H-7b, H-6b; H-6b with H-5, H-6a; H-6a with H-6b, H-7a; H-7a with H-6b, H-7b; H-7b with H-7a, N^9-CH_3 ; N^9-CH_3 with H-7b. ^{13}C-NMR ($CDCl_3$) δ; 10.58(C3-CH_3), 29.37(N9-CH_3), 32.4(3), 34.80 (2), 47.29 (1), 50.60 (4), 51.38 (5), 68.62 (8), 107.37 (C^6=CH_2), 147.07 (6), 154.11 (10), 167.10 (12). MS *m/z* (%):229 ([M-H]$^+$, 82), 215 (69), 190 (100), 172 (20), 158 (33),147 (75),144 (38), 129 (13), 119 (89), 91 (29). HRMS; Calcd for $C_{13}H_{13}N_2O_2$; 229.0977. Found; 229.0980.

9,11-Diaza-2,9-dimethyl-5-methylenepentacyclo[6.4.0.0^{1,3}.0^{2,6}.0^{4,8}]dodecane-10,12-dione (6c): colorless crystals. mp 172-174 °C (acetone-hexane).^{1}H-NMR ($CDCl_3$) δ; 1.57 (1H, d, *J*=9.8 Hz, H-7a), 1.62 (3H, s, C^2-CH_3), 1.75 (1H, dt, *J*=9.8, 2.3 Hz, H-7b), 2.70 (1H, brt, H-6), 2.80 (1H, t, *J*=2.3, 2.9 Hz, H-4), 2.86 (3H, s, N^9-CH_3), 2.89 (1H, d, *J*=2.9 Hz ,H-3), 4.53 (1H, s, C^5=CHb),4.64 (1H, s, C^5=CHa). NOE; C^2-CH_3 with H-6, H-3; H-4 with H-3, H-5b; H-5a with H-5b; H-6 with H-5a, H-7a , C^2-CH_3 ; H-7a with H-7b; H-7b with H-7a, N^9-CH_3; N^9-CH_3 with H-7b. ^{13}C-NMR ($CDCl_3$) δ; 12.43 (C^2-CH_3), 29.37 (N^9-CH_3), 40.17 (2), 41.76 (3), 45.78 (7), 46.21 (6), 46.25 (4), 48.67 (1), 65.86 (8), 98.45 (C^5=CH_2), 152.37 (10), 157.34 (5), 167.81 (12). MS *m/z* (%):230 (M^+, 7), 215 (100), 172 (59), 144 (26), 129 (5), 115 (9), 91 (18), 77 (9). HRMS; Calcd for $C_{13}H_{14}N_2O_2$; 230.1055. Found; 230.1055.

1, 6, 8, 10-Tetramethylcyclooctapyrimidine-2, 4-dione (4d): orange oil. ^{1}H-NMR (C_6D_6) δ; 1.79 (3H, s, C^8-CH_3), 1.81 (3H, s, C^6-CH_3), 1.90 (3H, s, C^{10}-CH_3), 3.27 (3H, s, N^1-CH_3), 5.61 (1H, s, H-7), 5.95 (1H, s, H-5), 5.97 (1H, s, H-9), 9.20 (1H, brs, N^3-H). NOE; C^{10}-CH_3 with N^1-CH_3, H-9; H-9 with C^{10}-CH_3, C^8-CH_3; C^8-CH_3 with H-9, H-7; C^6-CH_3 with H-7, H-5; N^1-CH_3 with C^{10}-CH_3 .^{13}C-NMR (C_6D_6) δ; 21.37 (C^{10}-CH_3), 22.55 (C^8-CH_3), 23.78 (C^6-CH_3), 32.52 (N^1-CH_3), 112.09 (4a), 120.07 (5), 129.91 (7), 131.76 (10), 135.21 (9), 137.22 (8), 142.06 (6), 151.97 (10a), 152.93 (2), 160.89 (4). MS *m/z* (%): 244 (M^+, 100), 229 (76), 201 (5), 186 (45), 173 (23), 158 (35), 144 (15), 129 (10). HRMS; Calcd for $C_{14}H_{16}N_2O_2$; 244.1212. Found; 244.1209.

9,11-Diaza-2,4,9-trimethyl-6-methylenepentacyclo[6.4.0.0^{1,3}.0^{2,5}.0^{4,8}]dodecane-10,12-dione (5d): colorless crystals. mp 231-233 °C (EtOH).^{1}H-NMR ($CDCl_3$) δ; 1.16 (3H, s, C^4-CH_3), 1.57 (3H, s, C^2-CH_3), 2.49 (1H, dt, *J*=16.7, 2.5 Hz, H-7b), 2.58 (1H, dt, *J*=16.7, 2.5 Hz, H-7a), 2.94 (3H, s, N^9-CH_3), 2.96 (1H, s, H-5), 3.33 (1H, s, H-3), 4.84 (1H, brs, C^6=CHb), 4.93 (1H, t, *J*=2.5 Hz, C^6=CHa), 7.32 (1H, brs, N^{11}-H). NOE; C^2-CH_3 with H-5, H-3; H-3 with C^2-CH_3, C^4-CH_3; C^4-CH_3 with H-3, H-5, N^9-CH_3; H-6a with H-6b, N^9-CH_3 ; N^9-CH_3 with H-7a, C^4-CH_3. ^{13}C-NMR ($CDCl_3$) δ; 11.10 (C^2-CH_3), 14.44 (C^4-CH_3), 30.24 (1), 30.44 (N^9-CH_3), 34.99 (7), 38.74 (2), 44.78 (3), 56.46 (4), 62.63 (5), 70.77 (8), 108.31 (C^6=CH_2), 145.03 (6), 154.42 (10), 168.04 (12). MS *m/z* (%):243 ([M-H]$^+$, 13), 229 (100), 204 (24), 186 (29), 172 (20), 158 (45), 133 (29), 117 (18). HRMS; Calcd for $C_{14}H_{16}N_2O_2$; 244.1212. Found; 244.1194.

9, 11-Diaza-3, 7, 9-trimethyl-5-methylenepentacyclo[6.4.0.0^{1,3}.0^{2,6}.0^{4,8}]dodecane-10, 12-dione (6d): colorless crystals. mp 181-183 °C (acetone-hexane).^{1}H-NMR ($CDCl_3$) δ; 0.84 (3H, d, *J*=6.3 Hz, C^7-CH_3), 1.41 (3H, s, C^3-CH_3), 1.97 (1H, brq, *J*=6.3 Hz, H-7), 2.64 (1H, m,H-6), 2.74 (1H, m, H-2), 2.81 (3H, s, N^9-CH_3), 2.94 (1H, s, H-4), 4.50 (1H, s, C^5=CHa), 4.61 (1H, s, C^5=CHb). NOE; C^3-CH_3 with H-2, H-6 ; H-5a with H-6 , H-5b; H-5b with H-5a, H-6; H-6 with H-5a, H-5b, H-4, H-2, N^9-CH_3,

C^3-CH_3, C^7-CH_3; C^7-CH_3 with H-7, H-6, N^9-CH_3; N^9-CH_3 with H-6, H-7. ^{13}C-NMR ($CDCl_3$) δ; 8.43 (C^7-CH_3), 12.62 (C^3-CH_3), 29.60 (N^9-CH_3), 39.83 (2), 46.61 (6), 47.83 (3), 50.52 (4), 50.65 (1), 51.36 (7), 66.31 (8), 98.35 (C^5=CH_2), 153.13 (10), 156.44 (5), 167.21 (12). MS *m/z* (%):244 (M^+, 56), 229 (100), 201 (14), 200 (11), 186 (51), 173 (9), 158 (39), 144 (9), 129 (12), 116 (8). HRMS; Calcd for $C_{14}H_{16}N_2O_2$; 244.1212. Found; 244.1216.

ACKNOWLEDGMENTS

This work has been supported in part by "Academic Frontier" Project from the Ministry of Education, Culture, Sports, Science and Technology of Japan.

REFERENCES

1. M. D. Shetlar, *Photochem. Photobiol. Rev.*, 1980, **5**, 105; T. Matsuura, I. Saito, H. Sugiyama, and T. Shinmura, *Pure Appl. Chem.*, 1980, **52**, 2705.
2. K. Seki, N. Kanazashi, and K. Ohkura, *Heterocycles*, 1991, **32**, 229; K. Ohkura, K. Kanazashi, and K. Seki, *Chem. Pharm. Bull.*, 1993, **41**, 239.
3. K. Ohkura, Y. Noguchi, and K. Seki, *Heterocycles*, 1997, **46**, 141; K. Ohkura, Y. Noguchi, and K. Seki, *Heterocycles*, 1998, **47**, 429; K. Ohkura, Y. Noguchi, and K. Seki, *Heterocycles*, 1998, **49**, 59.
4. K. Ohkura, K. Nishijima, A. Sakushima, and K. Seki, *Heterocycles*, 2000, **53**, 1247; K. Ohkura, K. Nishijima, S. Uchiyama, A. Sakushima, and K. Seki, *Heterocycles*, 2001, **54**, 65; K. Ohkura, K. Nishijima, S. Uchiyama, A. Sakushima, and K. Seki, *Heterocycles*, 2001, **55**, 1015.
5. K. Ohkura and K. Seki, *Photochem. Photobiol.*, 2002, **75**, 579.
6. K. Ohkura, N. Kanazashi, K. Okamura, T. Date, and K. Seki, *Chem. Lett.* **1993**, 667; K. Ohkura, K. Seki, H. Hiramatsu, K. Aoe, M. Terashima, *Heterocycles*, 1997, **44**, 467.
7. K. Ohkura, K. Nishijima, and K. Seki, *Chem. Pharm. Bull.*, 2001, **49**, 384; K. Ohkura, K. Nishijima, and K. Seki, *Photochem. Photobiol.*, 2001, **74**, 385.

Available online at www.sciencedirect.com
SCIENCE DIRECT®
Tetrahedron Letters
Tetrahedron Letters 47 (2006) 5321–5323

A new convenient method for the synthesis of [2-^{11}C]thymine utilizing [^{11}C]phosgene

Kazue Ohkura,[a,*] Ken-ichi Nishijima,[a] Kimihito Sanoki,[a] Yuji Kuge,[b] Nagara Tamaki[b] and Koh-ichi Seki[b,*]

[a]*Faculty of Pharmaceutical Sciences, Health Sciences University of Hokkaido, Ishikari-Tobetsu, Hokkaido 061-0293, Japan*
[b]*Graduate School of Medicine, Hokkaido University, Kita-15, Nishi-7, Kita-ku, Sapporo 060-8638, Japan*

Received 4 April 2006; revised 18 May 2006; accepted 19 May 2006
Available online 13 June 2006

Abstract—β-(*N*-Benzoylamino)methacrylamide, a key intermediate for the preparation of [2-^{11}C]thymine, was synthesized in three steps from ethyl α-formylpropionate and NH_3. Reaction of the alkali metal salts of β-(*N*-benzoylamino)methacrylamide with [^{11}C]phosgene gave [2-^{11}C]thymine. The yield of [2-^{11}C]thymine was 362 ± 53 MBq at EOS ($n = 3$) (18 MeV proton beam; 10 μA, 10 min). The total synthesis was accomplished in just 16 min from the end of bombardment.

Uracil derivatives are of considerable interest because of their wide array of pharmacological properties, and many pyrimidine-based radiopharmaceuticals have been developed for clinical diagnosis in the field of single photon or positron emission computed tomography.[1] The search for new or improved synthetic routes leading to labeled thymidine for evaluation of cellular proliferation by positron emission tomography (PET) has attracted much attention in recent years. Because of the short-lived positron emitting radionuclide (ca. ^{11}C: 20.4 min, ^{13}N: 10.0 min, ^{15}O: 2.0 min, respectively) and the radioactive level, a very rapid and simple labeling process with an efficient organic reaction and an automated synthesis apparatus to avoid radiation exposure are essential conditions for PET radiotracer synthesis.

In 1991, Vander Borght et al. synthesized [2-^{11}C]thymidine from [2-^{11}C]thymine formed via cyclocondensation of diethyl β-methyl malate with [^{11}C]urea.[2] Although other investigators have attempted to improve this method or develop related methodologies, the key ring closure reactions have traditionally relied on the condensation of a malate intermediate with the labeling agent [^{11}C]urea derived from phosgene,[2,3] cyanide,[4] or carbon dioxide.[5] Typically the reactions are carried out under as drastic conditions as those employed for ^{14}C labeled thymine synthesis.[6] The complexity of the currently available synthetic routes along with the extended length of preparation time has limited the extensive applicability of ^{11}C labeled nucleosides in PET studies.

Recently, we have developed a simplified and highly efficient synthesis of [^{11}C]$COCl_2$ with high specific activity.[7] ^{11}C labeled phosgene is a high-potency agent for the introduction of a ^{11}C carbonyl group to form versatile heterocyclic compounds as well as a variety of ureas. We have explored the utility of [^{11}C]$COCl_2$ for producing high-specific activity [^{11}C]CGP-12177, a radioligand for β-adrenoreceptors in the field of clinical PET.[8] This work has now prompted us to apply [^{11}C]$COCl_2$ in a ring closure step that would provide an efficient synthesis of [2-^{11}C]thymine.

We have designed alternative precursors as sources for the carbon skeleton that can be cyclocondensed with [^{11}C]$COCl_2$ to form the desired [2-^{11}C]thymine. Our strategy for the synthesis of [2-^{11}C]thymine is depicted in Scheme 1, wherein the key intermediate is β-aminomethacrylamide derivative (**1**). We now report herein a facile synthesis of [2-^{11}C]thymine by the direct condensation of [^{11}C]$COCl_2$ with the novel intermediate (**1**).

Keywords: [^{11}C]phosgene; [2-^{11}C]thymine; Positron emission tomography; β-(*N*-Benzoylamino)methacrylamide.
Abbreviations: EOS, end of synthesis; EOB, end of bombardment; PET, positron emission tomography; DME, 1,2-dimethoxyethane.
* Corresponding authors. Tel./fax: +81 1332 3 1267 (K.O.); e-mail: ohkura@hoku-iryo-u.ac.jp

0040-4039/$ - see front matter © 2006 Elsevier Ltd. All rights reserved.
doi:10.1016/j.tetlet.2006.05.143

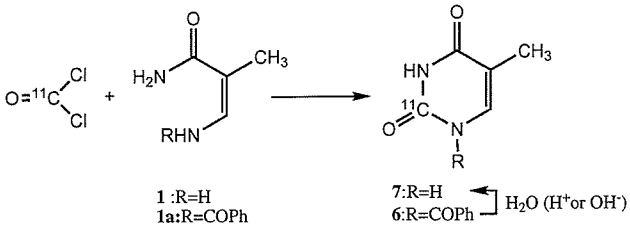

Scheme 1. Synthetic route of [2-^{11}C]thymine.

We have attempted to prepare the novel precursor β-aminomethacrylamide derivative (**1**), which leads to thymine or 1-acylated thymines by condensation reaction with phosgene. Previously, it had been reported that 1-acetylated or benzoylated thymine derivatives are rapidly hydrolyzed in ca. 20 s to produce thymine (Scheme 1).[9]

The key intermediate (**1**) was synthesized from β-aminomethacrylate (**3**) formed by the reaction of ethyl α-formylpropionate (**2**)[10] with NH_3. With the intent to activate the ester for producing amide, **3** was benzoylated prior to treatment with NH_3.

Treatment of the resulting compound (**4**) with NH_3 exclusively afforded β-(*N*-benzoylamino)methacrylamide (**1a**) without any detectable formation of the hydrolyzed product β-aminomethacrylamide (**1**, R = H) (Scheme 2). Attempts at the hydrolysis of benzoylated compound (**1a**) did not give **1**, hence, we examined the ring closure reaction using β-(*N*-benzoylamino)methacrylamide (**1a**).[11]

Synthesis of cold thymine was examined with **1a** by using triphosgene, which can be easily handled as a safe and stable replacement for phosgene. In order to accomplish the desired cyclocondensation, **1a** was activated as its alkali-metal salt. Addition of triphosgene to the sodium salt in DMF followed by hydrolysis gave thymine quantitatively.[12]

^{11}C labeled thymine production was achieved by using the same automated synthesis system as used for [^{11}C]CGP production from [^{11}C]$COCl_2$.[8] [^{11}C]$COCl_2$ was synthesized from [^{11}C]methane via [^{11}C]CCl_4 according to our previously reported method.[7] [^{11}C]methane was produced using an ultracompact cyclotron by the ^{14}N (p, α) ^{11}C nuclear reaction on nitrogen containing hydrogen (5%) in an aluminum target. Bombardment was carried out with a 10 μA beam of 18 MeV protons for 10 min.

The direct ring closure reaction of [^{11}C]$COCl_2$ possessing superior reactivity with non-activated precursor (**1a**) was first examined, but this approach failed to give the target product. Thymine precursor (**1a**), which was activated as the alkali metal salt (**5a**,**b**) reacted with [^{11}C]$COCl_2$ as well as triphosgene to afford [2-^{11}C]thymine (Scheme 3). The best result was obtained when the reaction was performed with potassium salt (**5b**) in DME as shown in Table 1.[13] The yield of [2-^{11}C]thymine under these conditions was 362 ± 53 MBq at EOS ($n = 3$). The radiochemical yield of [2-^{11}C]thymine was ca. 27% from [^{11}C]$COCl_2$.[14] The [2-^{11}C]thymine produced was identified by co-chromatography with authentic thymine and found to be radiochemically homogeneous by HPLC. Additionally, it was confirmed by subsequent enzymatic conversion to [2-^{11}C]thymidine.[3,15] Thus our method, which utilizes the reaction of [^{11}C]$COCl_2$ with the appropriate activated precursor is a viable approach to providing an adequate supply of [2-^{11}C]thymine, reliably and reproducibly, for clinical PET tracer studies with [2-^{11}C]thymidine.

In all previous reports, labeling of the 2-position of thymine was accomplished by condensation of [^{11}C]urea and malate at 130 °C in fuming sulfuric acid. Recently, Steel et al. reported an improved method for the preparation of [2-^{11}C]thymine via a multi-step process using [^{11}C]urea derived from [^{11}C]$COCl_2$. This radiosynthesis of [2-^{11}C]thymine took approximately 30 min from EOB and the yield was 38.5% from [^{11}C]$COCl_2$.[3]

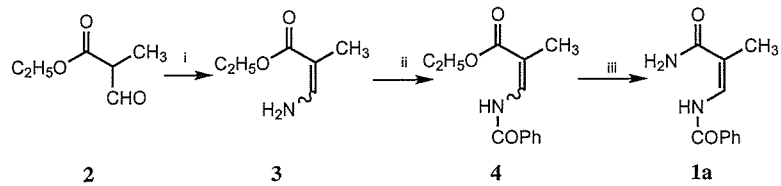

Scheme 2. Synthesis of β-(*N*-benzoylamino)methacrylamide (**1a**). Reagents and conditions: (i) NH_3, CH_3OH, reflux, 2 h; (ii) PhCOCl, C_5H_5N, $CHCl_3$; (iii) NH_3, CH_3OH.

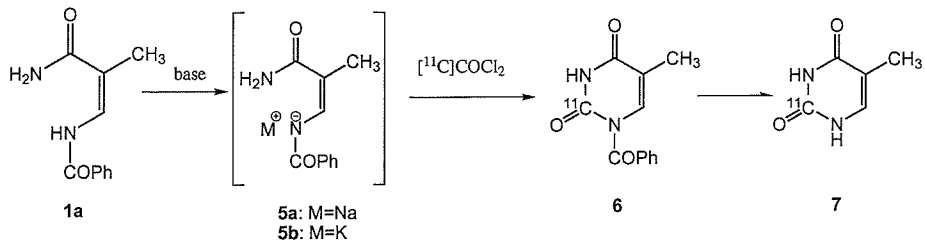

Scheme 3. Synthesis of [2-^{11}C]thymine (**7**).

Table 1. Yields of [2-^{11}C]thymine (7)

Solvent	Base	Mol equiv	Yield (MBq, EOS)
DME	—	—	ND
Toluene	NaH	5	41 ($n = 2$)
DME	NaH	2	68 ± 65 ($n = 3$)
DME	$(CH_3)_3COK$	2	137 ($n = 2$)
DME	$(CH_3)_3COK$	1	362 ± 53 ($n = 3$)

EOS: end of synthesis. ND: not detected. DME: 1,2-dimethoxyethane.

Although previous synthesis of [2-^{11}C]thymine via [^{11}C]urea is more efficient, our strategy involving the cyclocondensation with [^{11}C]$COCl_2$ for the direct production of [2-^{11}C]thymine is operationally simple, and offers fewer reaction steps at lower temperature. The total synthesis described herein takes 16 min from EOB to isolation of **7**, thus significantly shortening the reaction time, which is a crucial consideration for the preparation of short half-life radiopharmaceuticals.

In conclusion, we have provided a substantially useful method for the synthesis of [2-^{11}C]thymine. Having several merits over hitherto known methods, that is fewer reaction steps, mild reaction conditions, reliability of product yield, and simplified operations and synthetic instruments, the present methodology should find wide application in the preparation of many ^{11}C labeled radiopharmaceuticals. Extension of this method to the synthesis of other uracils and nucleosides is currently under investigation in our laboratory.

Acknowledgments

This study was supported in part by Grants-in-Aid for General Scientific Research and 'Academic Frontier' Project from the Ministry of Education, Culture, Sports, Science and Technology of Japan.

References and notes

1. Toyohara, J.; Fujibayashi, Y. *Nucl. Med. Biol.* **2003**, *30*, 681–685, and references cited therein.
2. Vander Borght, T.; Labar, D.; Pauwels, S.; Lambotte, L. *Int. J. Appl. Radiat. Isot.* **1991**, *42*, 103–104.
3. Steel, C. J.; Brady, F.; Luthra, S. K.; Brown, G.; Khan, I.; Poole, K. G.; Sergis, A.; Jones, T.; Price, P. M. *Appl. Radiat. Isot.* **1999**, *51*, 377–388.
4. Link, J. M.; Grierson, J. R.; Krohn, K. A. *J. Label. Compd. Radiopharm.* **1995**, *37*, 610–612.
5. Chakraborty, P. K.; Mangner, T. J.; Chugani, H. T. *Appl. Radiat. Isot.* **1997**, *48*, 619–621.
6. Vander Borght, T.; Pauwels, S.; Lambotte, L.; De Saeger, C.; Beckers, C. *J. Label. Compd. Radiopharm.* **1990**, *28*, 819–822.
7. Nishijima, K.; Kuge, Y.; Seki, K.; Ohkura, K.; Motoki, N.; Nagatsu, K.; Tanaka, A.; Tsukamoto, E.; Tamaki, N. *Nucl. Med. Biol.* **2002**, *29*, 345–350.
8. Nishijima, K.; Kuge, Y.; Seki, K.; Ohkura, K.; Morita, K.; Nakada, K.; Tamaki, N. *Nucl. Med. Commun.* **2004**, *25*, 845–849.
9. Cruickshank, K. A.; Jiricny, J.; Reese, C. B. *Tetrahedron Lett.* **1984**, *25*, 681–684.
10. Marx, J. N.; Craig Argyle, J.; Norman, L. R. *J. Am. Chem. Soc.* **1974**, *96*, 2121–2129.
11. Selected data **1a**: (*Z*)-β-(*N*-Benzoylamino)methacrylamide: mp 182–184 °C (recrystallized from 50% AcOEt–hexane). ^{1}H NMR ($CDCl_3$): δ 1.95 (3 H, d, $J = 1.2$ Hz), 5.40–5.80 (2H, br d, D_2O exchangeable, NH_2), 7.46 (2H, t, $J = 7.2$ Hz), 7.54 (1H, t, $J = 7.2$ Hz), 7.54 (1H, d, $J = 7.5$ Hz), 7.93 (2H, d, $J = 7.2$ Hz), 12.3 (1H, br s, D_2O exchangeable, NH). Anal. Calcd for $C_{11}H_{12}N_2O_2$: C, 64.69; H, 5.92; N, 13.72. Found: C, 64.50; H, 6.05; N, 13.60.
12. The chemical purity of the product isolated by HPLC was 99%. Spectroscopic data (NMR, IR, and MS) of the product were completely superimposable on those of authentic thymine.
13. [^{11}C]$COCl_2$ was bubbled with helium flow into a reaction vial containing a solution of **5b** (0.2 mg) in DME (0.5 mL) in the presence of the base at 30 °C for 1 min. After removal of the solvent, treatment of the residual [2-^{11}C]*N*-benzoylthymine (**6**) with 1.5 M ammonia–methanol for 1 min at room temperature resulted in debenzoylation to yield **7**. The reaction mixture was subjected to reverse-phase HPLC equipped with UV monitor and γ counter (μ-Bondapak C_{18}, 25 cm × 0.39 cm i.d., 3% EtOH–Saline, flow rate 0.5 mL/min at 40 °C). The radioactive peak at 11 min was the desired [2-^{11}C]thymine. The product was observed to be 99% radiochemically pure by HPLC.
14. The yield of [2-^{11}C]thymine was determined based on produced [^{11}C]$COCl_2$. We estimated the yield of [^{11}C]$COCl_2$ to be about 1500 MBq based on the yield of diphenylurea.
15. Friedkin, M.; Roberts, D. *J. Biol. Chem.* **1954**, *207*, 257–266.

Development of a novel fluorescent imaging probe for tumor hypoxia by use of a fusion protein with oxygen-dependent degradation domain of HIF-1α

Shotaro Tanaka[a, b], Shinae Kizaka-Kondoh*[a, b, c], Hiroshi Harada[a], & Masahiro Hiraoka[a, b]
[a] Department of Radiation Oncology and Image-applied Therapy, Kyoto University Graduate School of Medicine. 54 Kawahara-cho, Shogoin, Sakyo-ku, Kyoto, 606-8507 Japan. Phone/FAX: +81-75-751-4242; [b] Kyoto City, Collaboration of Regional Entities for the Advancement of Technological Excellence, Japan Science and Technology Agency. Creation Core Kyoto Mikuruma、448-5 Kajiicho, Kamigyo-ku, Kyoto Japan; [c] COE Formation for Genomic Analysis of Disease Model Animals with Multiple Genetic Alterations, Kyoto University Graduate School of Medicine. 54 Kawahara-cho, Shogoin, Sakyo-ku, Kyoto, Japan.

ABSTRACT

More malignant tumors contain more hypoxic regions. In hypoxic tumor cells, expression of a series of hypoxia-responsive genes related to malignant phenotype such as angiogenesis and metastasis are induced. Hypoxia-inducible factor-1 (HIF-1) is a master transcriptional activator of such genes, and thus imaging of hypoxic tumor cells where HIF-1 is active, is important in cancer therapy. We have been developing PTD-ODD fusion proteins, which contain protein transduction domain (PTD) and the VHL-mediated protein destruction motif in oxygen-dependent degradation (ODD) domain of HIF-1 alpha subunit (HIF-1α). Thus PTD-ODD fusion proteins can be delivered to any tissue *in vivo* through PTD function and specifically stabilized in hypoxic cells through ODD function. To investigate if PTD-ODD fusion protein can be applied to construct hypoxia-specific imaging probes, we first constructed a fluorescent probe because optical imaging enable us to evaluate a probe easily, quickly and economically in a small animal. We first construct a model fusion porein PTD-ODD-EGFP-Cy5.5 named POEC, which is PTD-ODD protein fused with EGFP for in vitro imaging and stabilization of fusion protein, and conjugated with a near-infrared dye Cy5.5. This probe is designed to be degraded in normoxic cells through the function of ODD domain and followed by quick clearance of free fluorescent dye. On the other hand, this prove is stabilized in hypoxic tumor cells and thus the dye is stayed in the cells. Between normoxic and hypoxic conditions, the difference in the clearance rate of the dye will reveals suited contrast for tumor-hypoxia imaging. The optical imaging probe has not been optimized yet but the results presented here exhibit a potential of PTD-ODD fusion protein as a hypoxia-specific imaging probe.

Keywords: Tumor hypoxia, Near-infrared (NIR) fluorescent imaging, Oxygen-dependent degradation (ODD), Hypoxia-inducible Factor (HIF)-1α, Protein Transduction Domain (PTD)

1. INTRODUCTION

Solid tumors often contain hypoxic regions with reduced oxygen tension far below physiological levels (1). Detecting hypoxic regions in tumor is very important for cancer therapies because of the following reasons; 1) Hypoxic regions are formed as a consequence of rapid tumor growth and profoundly disorganized vasculature (1-3); 2) Hypoxic tumor cells are resistant to radiotherapy and chemotherapy (2); 3) In hypoxic tumor cells, hypoxia-inducible transcriptional factors, such as HIF-1, induce various hypoxia-responsive genes, which confer malignant phenotypes of tumors such as apoptosis resistance, tumor growth, invasion and metastasis (2-4) and thus HIF-1 expression is closely associated with malignancy and poor prognosis; 4) Hypoxic region is detected in experimental tumors less than 1 mm in diameter.

Genetically Engineered and Optical Probes for Biomedical Applications IV, Samuel Achilefu, Darryl J. Bornhop, Ramesh Raghavachari, Alexander P. Savitsky, Rebekka M. Wachter, Eds., Proc. of SPIE Vol. 6449, 64490Y, (2007) · 1605-7422/07/$18 · doi: 10.1117/12.713633

HIF-1 is the major hypoxia-inducible transcription factor composed of α and β subunits (4-6). HIF-1α is regulated in an oxygen-dependent manner at the post-translational level (4, 5), while HIF-1β is constitutively expressed. HIF-1α contains oxygen-dependent degradation (ODD) domains (4, 5, 7) and is hydroxylated at proline residues in ODD domain by 4-prolyl hydroxylases (PHDs) (8, 9). The modification accelerates the interaction of the HIF-1α protein with the von Hippel-Lindau (VHL) tumor suppressor protein (10, 11), resulting in the rapid ubiquitination and subsequent degradation of the protein by the 26S proteasome (8-12). Thus oxygen-dependent regulation of HIF-1 activity is absolutely dependent on the stability of HIF-1α protein.

We have developed fusion proteins containing $ODD_{548\text{-}603}$, which has VHL-mediated protein destruction motif of HIF-1α and demonstrated that stability of the ODD fusion proteins are regulated by oxygen concentration as the same manner as HIF-1α (13). That is, the fusion proteins are rapidly degraded in normoxic cells and stabilized in hypoxic cells. Furthermore, we fused a protein transduction domain (PTD) to ODD fusion protein and demonstrated that resultant PTD-ODD fusion proteins are still under the same oxygen-dependent regulation as HIF-1α (13) and delivered to hypoxic cells in tumors (14-18).

Here we report a PTD3-ODD fusion protein as a novel probe for imaging hypoxic regions in tumors. PTD3 is a novel amphipathic one, which consists of poly-cathionic domain and hydrophobic domain. To evaluate the efficacy of PTD-ODD fusion protein as a hypoxia-specific probe, we conjugated a near infrared fluorescent (NIRF) dye Cy5.5 and examined bio-kinetics of the probe in tumor-bearing mice.

2. METHODOLOGY

2.1 Plasmid construction

The plasmids for preparing recombinant proteins EGFP, PTD3-ODD-EGFP and poly-Lysine (K9)-EGFP were constructed by inserting their encoding sequences to pGEX6P3 vector (GE healthcare Bio-Science Corp. Piscataway, NJ).The coding sequences of EGFP were obtained by PCR amplification with pEGFP vector (Chlontech Mountain View, CA) as a template. PTD3 (KKKKKKKKKETWWETWWETW), and K9 (KKKKKKKKK) coding sequences were constructed by annealing corresponding oligonucleotides. The DNA fragment encoding ODD was obtained from pGEX6P3-TAT-ODD-Procaspase-3 plasmid (14) by digesting it with *Bgl*II and *Kpn*I.

2.2 Cell culture and hypoxia-mimic treatment *in vitro*

HeLa/5HRE-Luc cells (17) were maintained at 37°C in 5% FBS-Dulbecco's modified Eagle medium (DMEM, Nacalai Tesque, Kyoto, Japan) supplemented with penicillin (100 units/ml) and streptomycin (100 μg/ml).

For hypoxia-mimic condition, cells were treated with medium and buffers containing $CoCl_2$ (final concentration at 100 μM), which inhibits the oxygen-dependent degradation function of 4-prolyl hydroxylases (8). To observe oxygen-dependent degradation of POEC, HeLa/5HRE-Luc ($1X10^5$) cells were cultured in 35-mm dish, washed twice with saline, and incubated with saline containing POEC (0.72 nM) in 30 min at 37 °C with/without $CoCl_2$. Then the cells were washed with PBS and harvested by trypsinization to analyze Cy5.5-fluorescence intensity by IVIS200™ imaging system (Xenogen Corp., Alameda, CA). Obtained images were analyzed by Living Image 2.50-Igor Pro 4.09A software ((Xenogen Corp., Alameda, CA). Each experiment was repeated four times.

2.3 Preparation of PTD3-ODD-EGFP-Cy5.5

Fusion protein PTD3-ODD-EGFP (POE), K9-EGFP and EGFP was prepared by the basically same method as described previously (14) and dissolved at the final concentration of 1.0 mg/ml in PBS (pH 8.0). The NIRF dye, Cy5.5-NHS (GE healthcare Bio-Science Corp.), was reacted with POE fusion protein for 1 hr at room temperature. Then the reacted solution was treated by desalting column (Sephadex G-50, GE healthcare Bio-Science Corp.) equilibrated PBS (pH 8.0) to remove non-labeled free dye. The eluting fraction of Cy5.5-labelled POE (PTD3-ODD-EGFP-Cy5.5; POEC) was concentrated to the final concentration of 1.0 mg/ml by ultrafiltration (Amicon Ultra 10k, Millipore, Bollerica, MA). The absorbance of 280 and 675 nm were measured, and efficiency of labeling was determined by following the manufacturer's instruction manual.

2.4 Trypsin-digestion and SDS-PAGE analysis

Trypsin-digestion of and SDS-PAGE were undertaken to identify Cy5.5-labeled region of POEC. Trypsine (2.5 mg/ml) 5 μl was added into 100 μl of POEC solution (1.0 mg/ml) and incubation in 30 min at room temperature. Finally, 5 μl of the product was applied on SDS-PAGE (15% aclylamide gel). After electrophoresis, the gel was analyzed by using IVIS200^{TM} imaging system for Cy5.5 fluorescence detection (Fig. 2A). The maximum excitation- and emission wavelength of POEC was measured by using fluorescent spectrometer RF-5300PC (SHIMADZU, Kyoto, Japan).

2.5 Assessment of membrane transduction activity by flow cytometric analysis

To evaluate the membrane transduction activity of the fusion proteins with various protein transduction domains, HeLa/5HRE-Luc cells (1 x 10^5/well) were seeded in a 24-well plate. The following day, the cells were washed 3 times with PBS (pH 7.5) and cultured in 200 μl of serum-free DMEM with a fusion protein (approximately 50 μg). The amount of fusion protein was adjusted based on the EGFP fluorescent intensity. After 30 min incubation in CO_2 incubator, the cells were washed 3 times with DMEM (without FBS), once with PBS containing 0.02% EDTA, and then treated with 200 μl of 0.25% trypsin-EDTA solution at 37 °C for 5 min, and added 1ml of 5%FBS-DMEM. The cells were harvested and washed with PBS (pH 7.5) at once. Finally, the cells were re-suspended in 300 μl of ice-cold PBS (pH 7.5) and kept on ice. In case of the experiments for ODD-fusion protein, the cells were treated with the reagents containing $CoCl_2$ (final concentration at 100 μM) to inhibit oxygen-dependent degradation of ODD-fusion proteins. The EGFP fluorescent intensity of the cells was determined by flow cytometric analysis using CELLQuest (Becton-Dickinson, Mountain View, CA).

2.6 Xenograftic tumor formation

Cell suspensions of HeLa/5HRE-Luc cells (1 x 10^6 cells / 100 μl of PBS) were inoculated subcutaneously in the left and right hind legs of 8-week-old male nude mice (BALB/c *nu/nu*; Japan SLC, Hamamatsu, Japan). The mice were used for experiments 2 weeks after implantation.

2.7 In vivo fluorescence and luciferase imaging

The tumor bearing mice were intravenously injected with fluorescent dye-labeled probes and certain time after injection they were applied to IVIS200^{TM} system. This system collects photons of light emitted from mice through corresponding fluorescence filters using the cooled charge-coupled device camera.

To detect bioluminescence from xenografts of HeLa/5HRE-Luc cells (17), tumor-bearing mice were intraperitoneally injected with 100 μl D-luciferin solution (10 mg/ml in PBS; Promega Corp., Madison, WI). Ten minutes later the mice were put in IVIS200^{TM} ((Xenogen Corp., Alameda, CA). During the imaging, the mice were kept under anesthesia with 2.5% of isoflurane gas in oxygen flow (1.5 L/min). Obtained images were analyzed by Living Image 2.50-Igor Pro 4.09A software ((Xenogen Corp., Alameda, CA).

3. RESULTS

3.1 Design of hypoxia-specific probe PTD3-ODD-EGFP-Cy5.5 (POEC)

To image hypoxic tumor cells *in vivo*, we constructed a model fusion protein PTD3-ODD-EGFP-Cy5.5 (POEC), which consists of four functional parts, PTD3, ODD, EGFP, and Cy5.5 (Fig. 1A). PTD3 is a novel amphipathic PTD which was constructed with poly-cathionic domain and hydrophobic domain. PTD3 was fused on POEC to delivery the probe into cytosol of whole cells in the body through cell membrane. ODD is a part of ODD domain (548-603) of HIF-1α (ref), which is the VHL-mediated protein destruction motif of HIF-1α so that they can be degraded rapidly in normoxic cells and stabilized in hypoxic cells (13). Enhanced green fluorescent protein (EGFP) functions as a carrier and an in vitro imaging. Cy5.5 is for *in vivo* imaging, whose fluorescence wavelengths (650-700 nm) are suit for *in vivo* imaging because of its high transmittance, low interference and non-invasive on tissue. POEC is designed as follows: In normoxia, Cy5.5 is released from POEC at the protein degradation and goes out directly of cells because of its small

molecular weight: In hypoxic cells, Cy5.5 is remained in the cells because POEC is stabilized. These differences of the Cy5.5 clearance speed between normoxic and hypoxic cells would make marked contrast, resulting in visualization of tumor hypoxia.

3.2 Evaluation of POEC in vitro

The labeling-efficiency of the prepared POEC with Cy5.5 was 1.38, which was calculated by using the values of absorbance with 280 nm and 678 nm. The excitation- and emission wavelength of POEC were 683.4 nm and 697.0 nm, respectively, which are slightly different from Cy5.5-NHS (675 nm and 694 nm). The Labeled PTD3-ODD-EGFP (POE) retained EGFP fluorescence. The result of gel filtration revealed that the probe was monomer at that condition (data not shown).

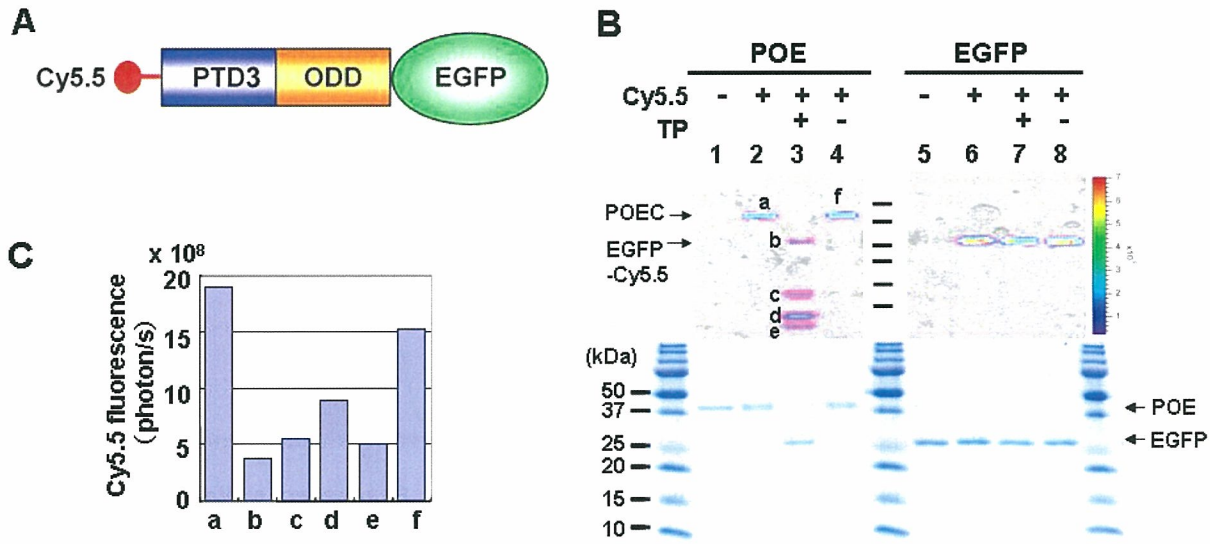

Fig. 1. Structural analysis of PTD3-ODD-EGFP-Cy5.5 (POEC). A. Diagram of POEC. B. Analysis of Cy5.5-labeling site. Purified PTD3-ODD-EGFP (left) and EGFP (right) were labeled with Cy5.5 (+; lanes 2-4 and 6-8 respectively) and digested with trypsin (TP +; lane 3 and 7 respectively), or untreated (lane 1 and 5, respectively). After electrophoresis, Cy5.5 fluorescent signal of the SDS-PAGE gel (15%) were detected by using IVIS200™ imaging system (upper panel) and then the gel was stained by CBB (lower panel). C. Cy5.5 fluorescent intensity. Fluorescence intensity of the Cy5.5-labeled polypeptides (a-f) in Figure 1B is shown in the graph.

3.2.1 Cy5.5-labeled domain

POEC was digested by trypsin to identify Cy5.5-labeled site. Trypsinized POEC was separated into four fragments: three smaller fragments (approximate molecular weight 5, 7 and 13 kDa) and the largest fragment with the same size as EGFP (approximate molecular weight: 27 kDa) (Fig. 1B, lower panel, lane 3). EGFP fluorescence intensity of the trypsinized POEC was similar to the one of undigested one (data not shown), indicating that EGFP domain was not digested by trypsin and that three smaller fragments were came from PTD-ODD domain. Cy5.5 fluorescence intensity analysis of SDS-PAGE gel demonstrated that while Cy5.5 fluorescence was observed on all the digested POEC fragments, about 83.7% of the total fluorescent intensity (the sum of b-e) was detected in PTD3-ODD region (fragment c-e) (Fig. 2B lower panel lane 3 and 2C). These results indicate that Cy5.5 was mainly located in PTD3-ODD domain. Because no lysine residue exists in the ODD domain and the labeling efficiency was nearly 1.0, Cy5.5 may mainly locate at N-terminal of PTD3 domain.

3.2.2 Membrane transduction activity

PTD function contributes in vivo delivery of PTD-fusion proteins (ref). Thus we evaluated membrane transduction activity of PTD3 after fused with ODD-EGFP and further labeled with Cy5.5. The membrane transduction activity of PTD-fusion proteins was examined by EGFP fluorescent intensity of the cells treated with PTD-fusion proteins: When higher membrane transduction activity PTD-fusion protein has, more EGFP fluorescent intensity the cells treated with it has. The cells treated with EGFP without PTD domain showed the same fluorescent intensity as untreated cells (data not shown). The cells treated with POE showed the similar fluorescent intensity to the ones treated with K9-EGFP, indicating that PTD3 has compatible membrane transduction activity as poly-Lysine (Fig. 2A).

Next we examined the influence of Cy5.5-labeling on the membrane transduction activity of PTD3 because the Cy5.5-labeling domain analysis indicated that Cy5.5-labeling site was mainly in PTD3 domain (Fig. 1A and 1B). The membrane transduction activity of POEC was slightly decreased compared to unlabelled POE (Fig. 2B), suggesting modification of PTD domain influence the PTD function. Although labeling with Cy5.5 slightly diminished the PTD ability of POE (Fig. 3B), the membrane transduction activity of PTD3 in POEC was still high.

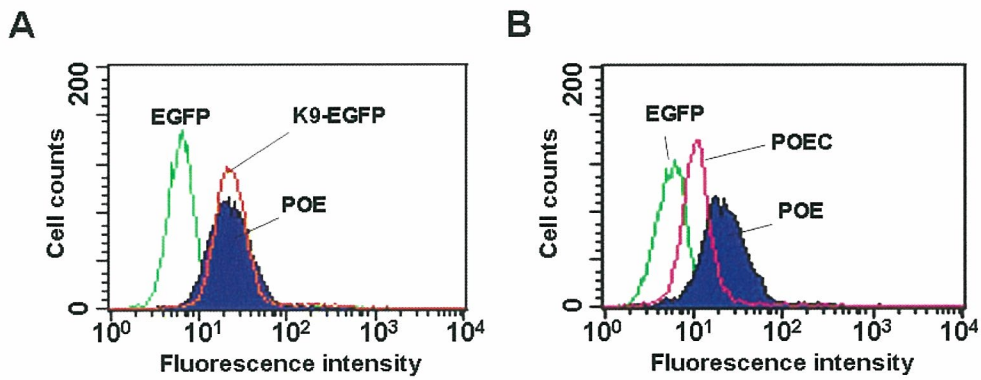

Fig. 2. FACS analysis of membrane transduction activity of PTD-fusion protein. EGFP or PTD-fusion proteins were added into the culture medium (serum-free DMEM) of HeLa/5HRE-Luc cells. After 30 min incubation in 37 °C, the cells were washed by PBS, trypsinized, and harvested and EGFP fluorescent intensity was analyzed with FACS. Each experiment was done in triplicate and repeated at least twice. A. EGFP, poly-Lysine (K9)-EGFP and POE were treated as described above and their EGFP fluorescent intensities are shown in graph. B. EGFP, POE and POEC were treated as described above and their EGFP fluorescent intensities are shown in graph.

3.2.3 Oxygen-dependent degradation of POEC in vitro.

Oxygen-dependent degradation regulation of POEC was examined by IVIS200™ imaging system. The cells were incubated with medium containing POEC with or without $CoCl_2$ and then Cy5.5 fluorescence intensity was examined with IVIS200™ imaging system (Fig. 3). Since the amount of stabilized POEC protein was very small, EGFP fluorescence of POEC was not detectable. On the other hand, the Cy5.5 fluorescence was sensitive enough to detect POEC (Fig. 3 right) because of their higher fluorescence intensity and longer residence time compared with EGFP. Under the same observation conditions, however, significantly less Cy5.5 fluorescence was observed in the cells treated without $CoCl_2$ (Fig.3 middle). Similar results were obtained by the experiment with other hypoxia-mimic reagent, FDG, which inhibits PHD2 by chelating Fe ions. These data demonstrate that the stability of POEC protein is regulated by PHD, thus oxygen concentration. No fluorescence was detected in any cells by the same experiment using Cy5.5-glycine (data not shown), suggesting small polypeptides labeled with Cy5.5 may easily go out of the cells.